

# NMTFD-2 Deliverable Task 1 Report: Numerical Investigations On Flow Over a Circular Cylinder

Onkar Marathe (23146448) onkar.marathe@fau.de  
Gokhul Shriram Ravi (23212226) gokhul.shriram.ravi@fau.de  
Adithya Umanath Rai (22811294) adithya.raai@fau.de

June 4, 2023

## Introduction:

The following study examines the flow around a cylinder. The task required us to design case studies and identify domain size and distances to the inlet, and outlet from the cylinder wall based on the Reynolds numbers. We were also tasked with generating grids with appropriate sizing and refinements. The choice of boundary conditions and initial conditions was also important in this task. The 3 Reynolds numbers selected were 100, 1600 and 3900 and information about our task will be discussed in the sections below.

## (I) Computational Domain and Boundary Conditions

The fluid Domain is illustrated in the figure with inflow, outflow and lateral distances indicated. The downstream length is set at 55D and kept larger than the upstream length, set at 15D, to accurately capture the vortex shedding phenomena (if applicable) for the aforementioned Reynolds Numbers. The lateral length is set at 2.5D. To accurately simulate the case, appropriate boundary conditions also have to be set at the inlet, outlet, walls and cylinder. The conditions are set as described in Table 1.

Table 1: Boundary Conditions

Parameters	Pressure	Velocity
Cylinder	Zero Gradient	Fixed Value - 0
Inlet	Zero Gradient	Fixed Value
Outlet	Zero	Zero Gradient
Top - Bottom Walls	Zero Gradient	Zero
Walls	Zero Gradient	Fixed Value - 0

## (II) Governing Equations and Solvers Used

The RANS equations give equations governing 3D turbulent incompressible isothermal flow. For this case, we use the RANS k- $\epsilon$  *model*.

In this model, 2 additional equations are solved along with the Mass and momentum conservation equations; an equation to calculate the turbulent kinetic energy and another equation to calculate turbulence dissipation. This model is suited for this particular case, however, this model is not ideal in the case of complex, unconfined and rotating flows. RANS Equations:

$$I = 0.16Re^{-0.125} \quad (1)$$

$$k = \frac{3}{2}v^2i \quad (2)$$

$$\epsilon = \frac{(C_\mu^{0.75})(k^{1.5})}{L} \quad (3)$$

$$L = 0.07D \quad (4)$$

Where  $I$  is the turbulence intensity,  $L$  is the turbulence length, and  $D$  is the diameter of the cylinder.

For our case, values are defined in the below tables.

Table 2: Parameters

$\nu$	<b>Re</b>	$\rho$	<b>v</b>	<b>Characteristic length</b>	$\mu$
$1.4115 * 10^{-5}$	100	1.293	0.003528	0.4	0.00001825
$1.4115 * 10^{-5}$	1600	1.293	0.056457	0.4	0.00001825
$1.4115 * 10^{-5}$	3900	1.293	0.137616	0.4	0.00001825

Table 3: Turbulent Properties

<b>I</b>	<b>k</b>	<b>Cmu</b>	<b>epsilon</b>	<b>Turbulent length</b>
0.089974	$1.5119 * 10^{-7}$	0.09	$3.45 * 10^{-10}$	0.028
0.0636216	$1.93531 * 10^{-5}$	0.09	$4.996 * 10^{-7}$	0.028
0.05691633	$9.20244 * 10^{-5}$	0.09	$5.1805 * 10^{-6}$	0.028

### (III) Meshing

#### **Grid Convergence Study:**

A grid convergence study is carried out to find out the discretization error in CFD simulations. This is done by simulating a case in successively finer grids. The solution is said to have converged if the difference in results between 2 successive grids approaches zero. In this case, a coarse grid containing X elements and a finer grid containing Y elements were used to study grid convergence. The drag force averaged over the entire domain is selected as the parameter of interest to show convergence. As the grid is refined (grid cells become smaller and the number of cells in the flow domain increase) and the time step is refined (reduced) the spatial and temporal discretization errors, respectively, should asymptotically approach zero, excluding computer round-off error. The grid convergence depends on various aspects of the grid; mainly non-orthogonality, skewness, aspect-ratio and smoothness.

#### **a) Non-Orthogonality**

Non-orthogonality is the angle between the face area vector and the cell centre to centre vector. Considerable errors are introduced by the diffusive term if the cells are non-orthogonal, therefore it is best to keep the value as low as possible. The ideal value for non-orthogonality is 0, and lower values of orthogonality introduce lesser errors, thereby improving convergence.

#### **b) Skewness**

Skewness is one of the primary quality measures for a mesh. Skewness determines how close to ideal (i.e., equilateral or equiangular) a face or cell is. The ideal value for skewness is 0, and the lower the value of skewness, the better the results for the simulation. OpenFOAM sets the maximum value of skewness at 4.

#### **c) Aspect Ratio**

Aspect ratio is defined as the ratio of a cell's maximum dimension to its minimum dimension. Large aspect ratios have to be avoided, as they do not capture gradients properly. This is especially true in areas where there is a rapid change of the divergence. Ideally, the aspect ratio has to be closer to 1, OpenFOAM sets the maximum for the aspect ratio at 1000.

#### **d) Smoothness**

Smoothness is defined as the difference between the largest cell volume and the smallest cell volume in the mesh. Sudden changes in the mesh size introduce errors during interpolation. To ensure that the mesh is smooth, it is important to make sure that the difference between the largest and the smallest volume is as low as possible, which physically means that the mesh becomes finer/coarser "gradually", thus introducing lesser errors while interpolation.

OpenFOAM sets the maximum threshold value for these parameters which can be checked by using the checkMesh command.

## (IV) pisoFoam

PisoFoam is a transient solver for incompressible, turbulent flow. PISO is a pressure-velocity calculation procedure for the Navier-Stokes equations, which is an extension of the SIMPLE algorithm. It involves first solving the momentum equation to estimate intermediate velocity and then solving the poisson equation to arrive at the pressure correction factor. Next, the pressure field and velocity fields are corrected and subsequently, the second poisson equation is solved to obtain the second pressure correction factor. The above steps are repeated with the updated values for pressure and velocity until the solution is obtained. The solution is said to be obtained if the values of correction factors of both the velocity and the pressure tend to be 0. Here, for solving the Task, we have used a considered time step size of 0.05 seconds.

### a) Iterations and Relaxation factor

Table 4: NCorrector and NOrthogonal correctors

NCorrector and NOrthogonal Value	Drag Value
1 and 1	95.7512
1 and 2	95.7371
2 and 1	96.9894
2 and 2	96.7985
3 and 2	96.8697
3 and 2 (mid)	100
3 and 2 (refined)	96.1754

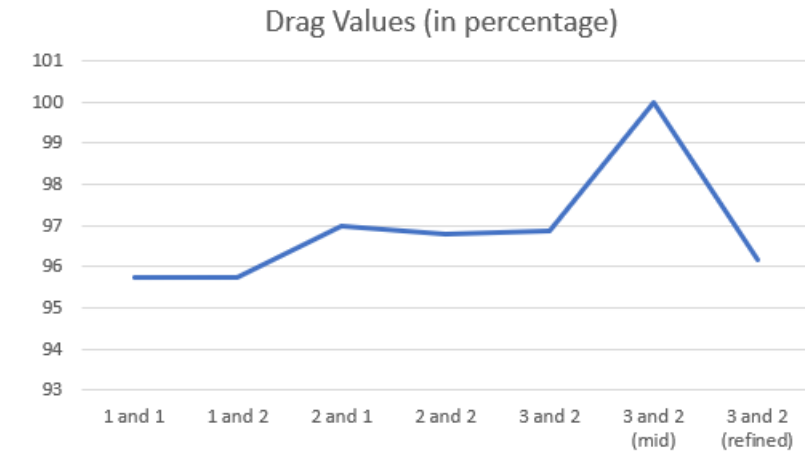


Figure 1: Graph for stability

### **b) Courant Number**

Special care has to be taken to make sure that the Courant number is low (ideally smaller than 1). The Courant number is a dimensionless constant which throws light on the rate at which information is transported per unit time step. For cases considered here, the Courant number is 0.002, 0.0323 and 0.08023 for the Re 100, Re 1600 and Re 3900 respectively. Also for refined cases, the Courant number is doubled as the mesh size is halved.

$$CourantNo. = u \frac{\Delta t}{\Delta x} \quad (5)$$

## **(V) Vortex Shedding**

### **a) Abstract**

Vortex shedding is a phenomenon that occurs when a fluid flows past a solid object, in our case a cylinder, resulting in the periodic formation and shedding of vortices in the wake of the object. It is a fluid dynamic instability that appears due to the interaction between the flowing fluid and the solid object. The governing equation regarding vortex shedding is also given by the following formula:

$$St = \frac{fd}{V} \quad (6)$$

Where  $St$  is the dimensionless Strouhal Number, describes oscillating flow mechanisms, and depends on the Re number.  $f$  is the vortex shedding frequency given in 1/s, and  $d$  is the diameter of the object through which the fluid passes past (in our case diameter of the cylinder) in m, and  $V$  is the velocity of the flow given in m/s.

### **b) Vortex Shedding Behavior at Various Renolds Numbers**

#### **i) Low Reynolds Numbers (Re<2000)**

At low Reynolds numbers, the flow is typically laminar and characterized by smooth and ordered fluid motion. In this flow, vortex shedding is not well-developed or even absent. The flow tends to be attached to the object's surface, and any vortices that form are small and quickly vanish. The absence of significant vortex shedding results in a relatively stable flow pattern. . It is also important to note that low Reynolds numbers is where we will observe creeping Flows (low Reynolds numbers,  $Re \ll 1$ ) and in creeping flows, the inertial forces are negligible compared to the viscous forces, and the flow is highly laminar.

As with the general observation for vortex shedding in low Reynolds numbers, vortex shedding is also not observed in creeping flows since the flow is too slow for the formation and shedding of vortices.

#### **ii) Transitional (Intermediate) Reynolds Numbers (2000<Re<4000)**

In this range, the flow may transition from laminar to turbulent. Vortex shedding can begin to occur, but it is not as well-defined or periodic as in higher Reynolds number flows. The shedding of vortices may be irregular and less predictable, leading to flow

fluctuations and intermittent vortex formation. This is the region of Reynolds numbers where we can begin to observe stable vortices. These vortices persist and maintain their coherence over time. The flow remains orderly, and vortex shedding is either absent or significantly suppressed. Stable vortices can occur when the flow is able to maintain a balance between the vorticity generation and dissipation, leading to the formation of coherent structures. As Reynolds number increases further, the flow can transition from stable vortices to a laminar vortex street. A laminar vortex street (Von Karman Street) is characterized by the regular shedding of vortices in the wake, resulting in a series of alternating vortices. This phenomenon is observed at higher Reynolds numbers, and the shedding frequency is related to the flow velocity and the object's dimensions. The vortices are shed in an orderly and periodic manner, creating a unique pattern.

### **iii) High Reynolds Numbers ( $Re > 4000$ )**

At higher Reynolds numbers, the flow becomes turbulent, characterized by chaotic and irregular fluid motion. Vortex shedding is well-established and periodic in this region. The shedding frequency and characteristics depend on the flow velocity, object geometry, and Reynolds number. The vortices shed in the wake can be large and coherent, leading to distinct flow patterns and pressure fluctuations. The alternating shedding of vortices can induce forces on the object, potentially causing vibrations or oscillations. In this region, the laminar vortex street can become unstable and transition to a turbulent vortex street. Turbulent flow is characterized by chaotic and irregular fluid motion. In this region, vortex shedding becomes more complex, and the vortices shed in the wake are smaller, less organized, and more randomly distributed. The flow exhibits turbulent fluctuations, increased mixing, and enhanced drag forces compared to laminar flows.

## (VI) Results

The impact of flow at different Reynolds numbers is significant on the flow characteristics and the occurrence of vortex shedding. Lower Reynolds numbers favor laminar or creeping flows with no or minimal vortex shedding. As the Reynolds number increases, stable vortices, laminar vortex streets, and turbulent vortex streets can arise, resulting in the periodic shedding of vortices with distinct flow patterns. The transition from laminar to turbulent flow affects the shedding frequency, the size and behaviour of the vortices, and the overall flow dynamics.

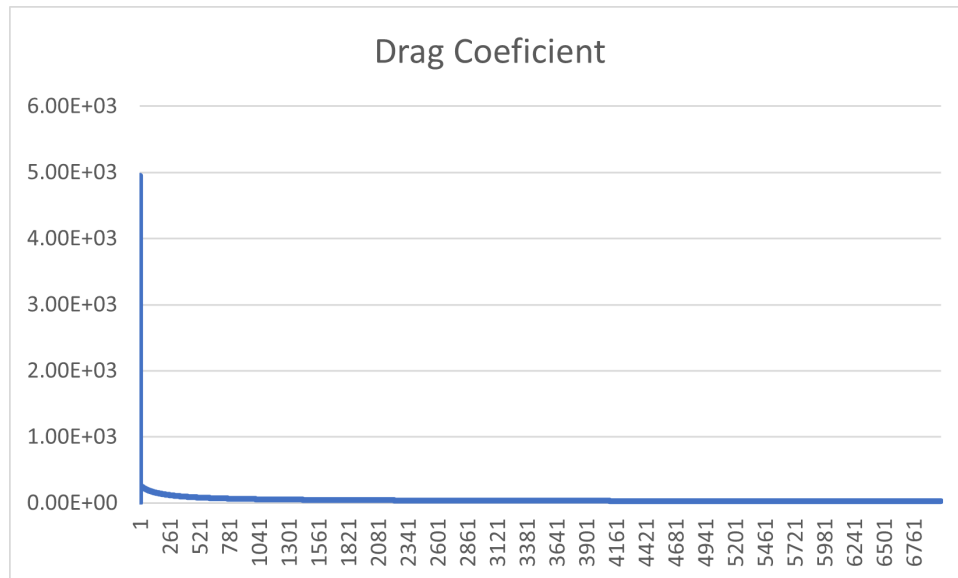


Figure 2: Drag Coefficient for Re 100

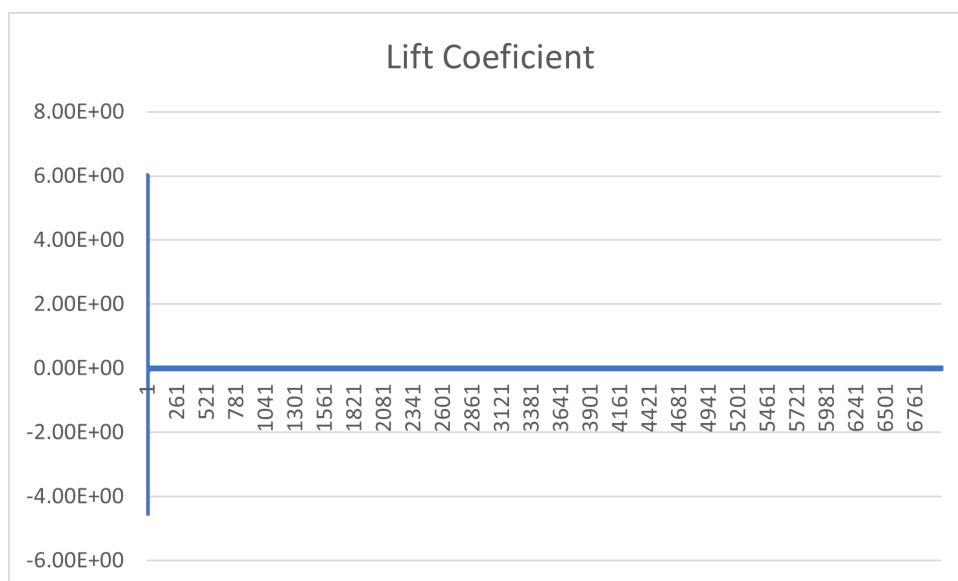


Figure 3: Lift Coefficient for Re 100

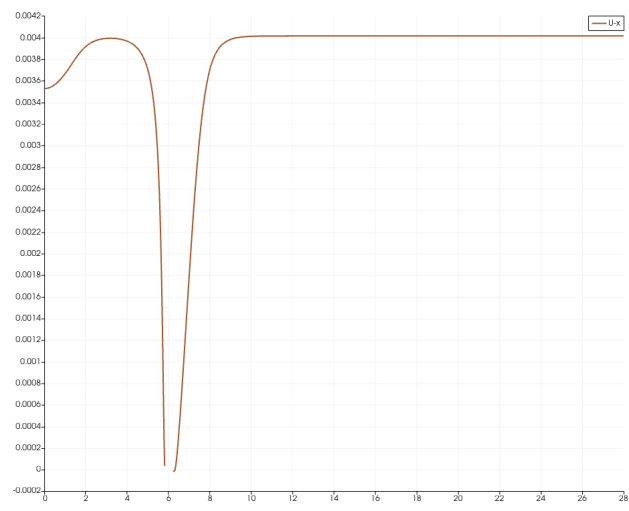


Figure 4:  $U_x$  for Re 100

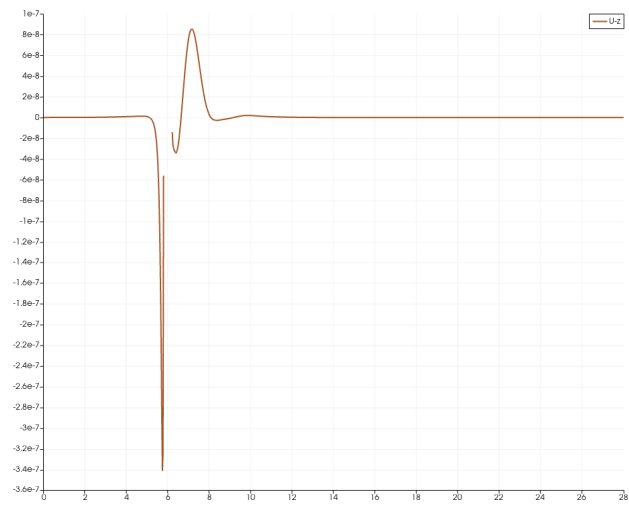


Figure 5:  $U_y$  for Re 100

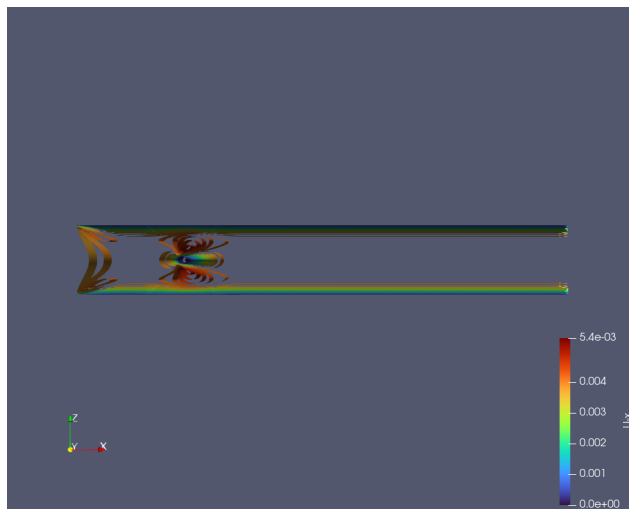


Figure 6:  $U_x$  Countour for Re 100



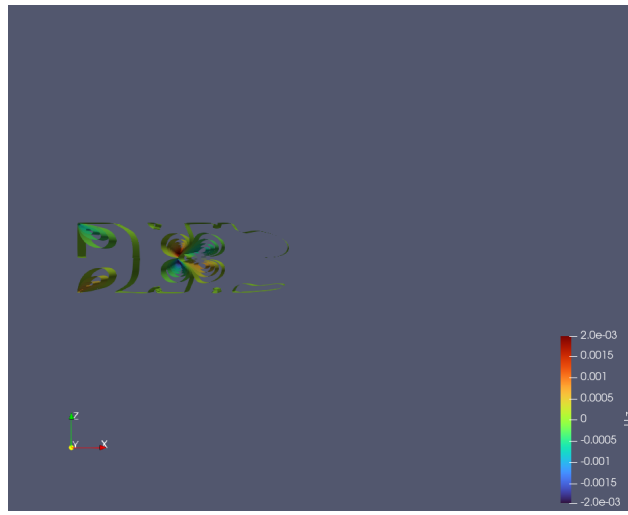


Figure 7: U-y Countour for Re 100

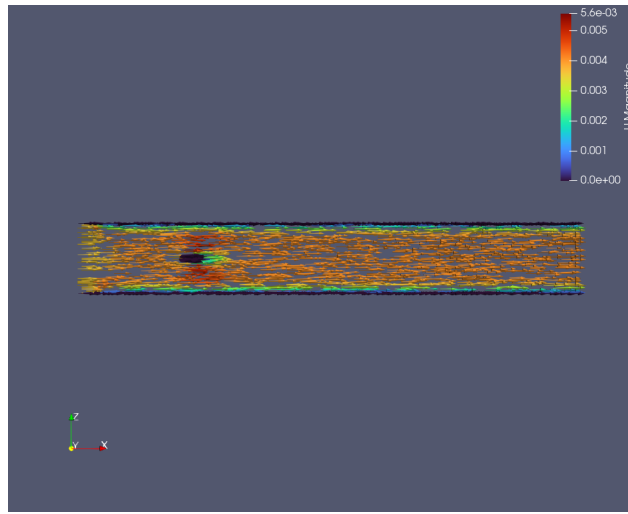


Figure 8: Vectors for Re 100

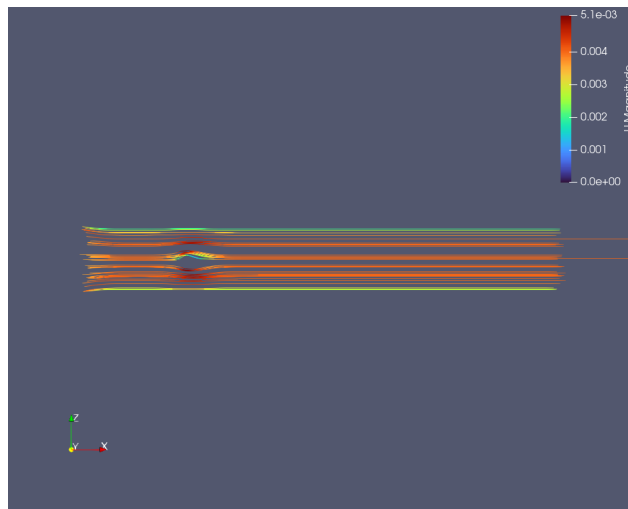


Figure 9: Streamlines for Re 100

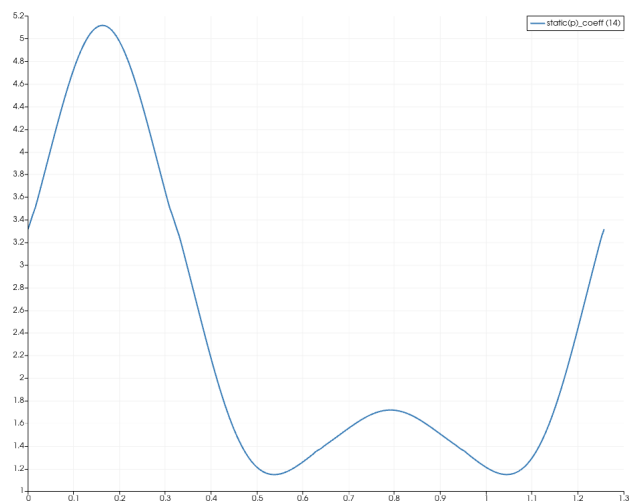


Figure 10: Pressure coefficient for Re 100

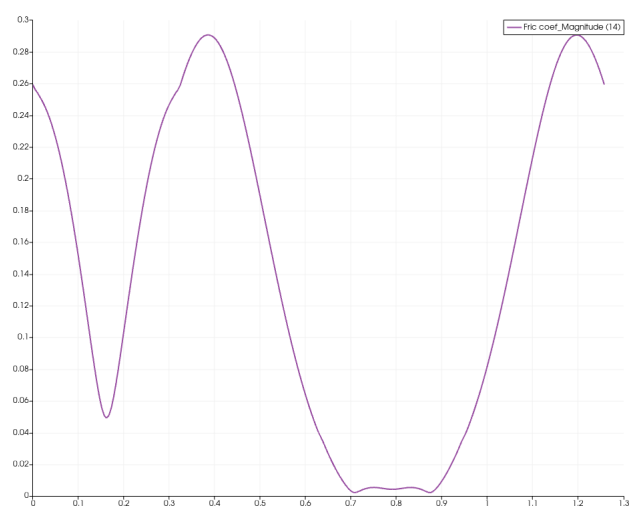


Figure 11: Friction Coefficient for Re 100

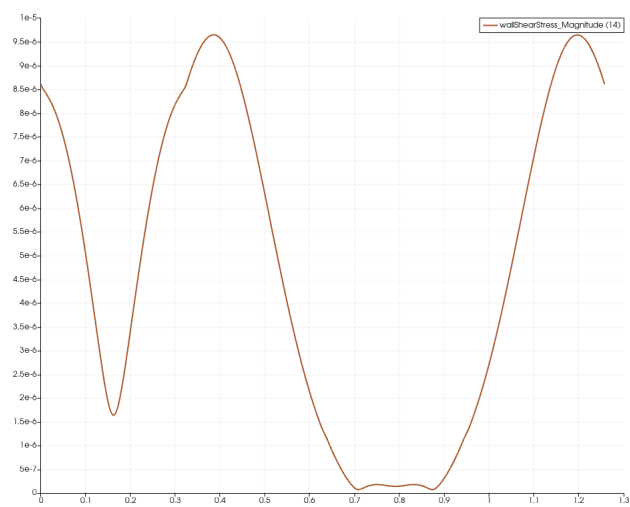


Figure 12: Wall Shear stress for Re 100

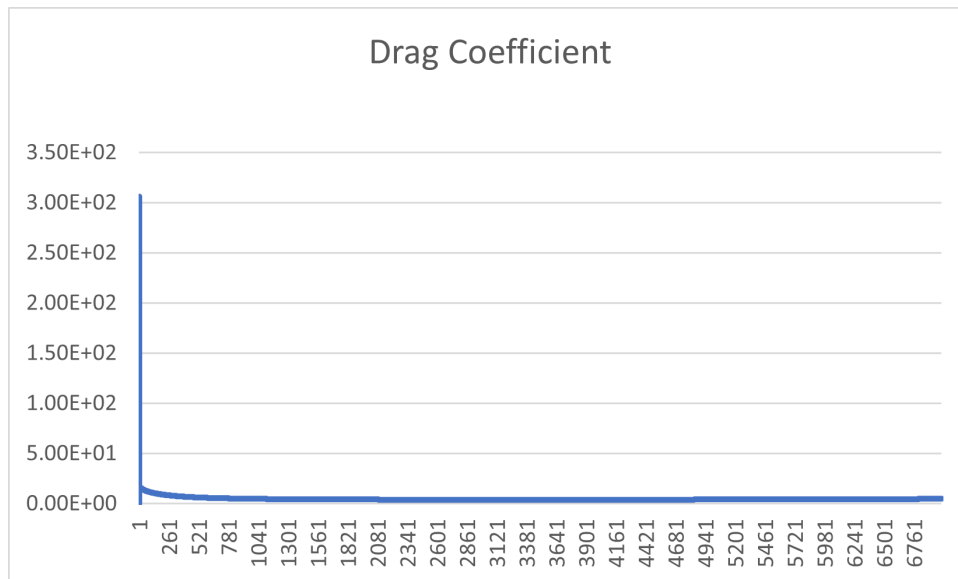


Figure 13: Drag Coefficient for  $Re = 1600$

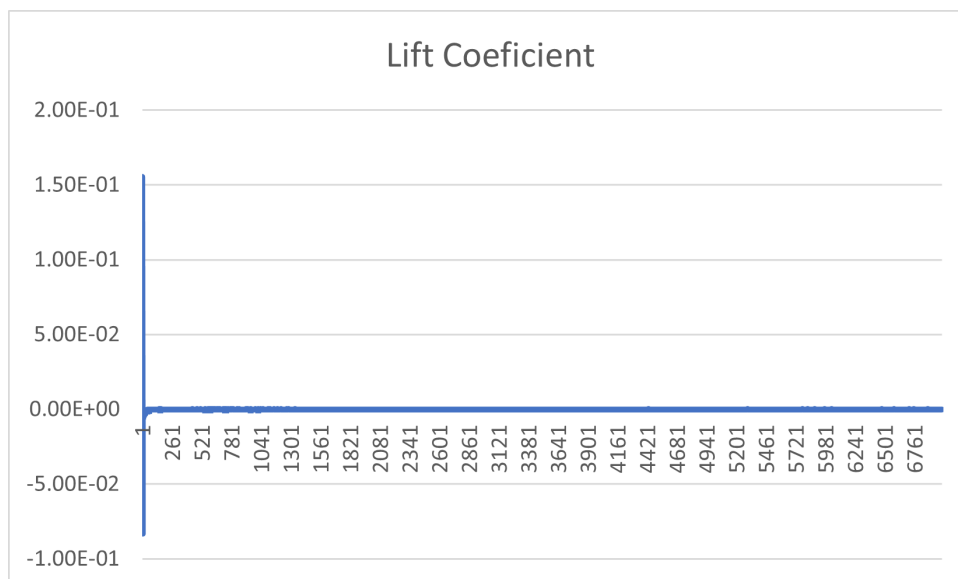


Figure 14: Lift Coefficient for  $Re = 1600$

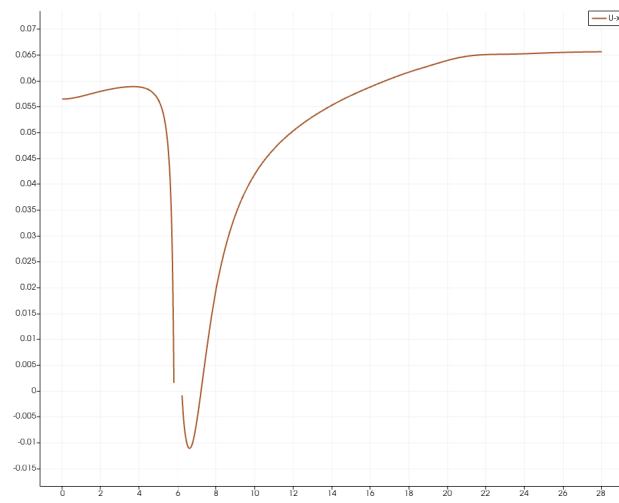


Figure 15:  $U-x$  for  $Re\ 1600$

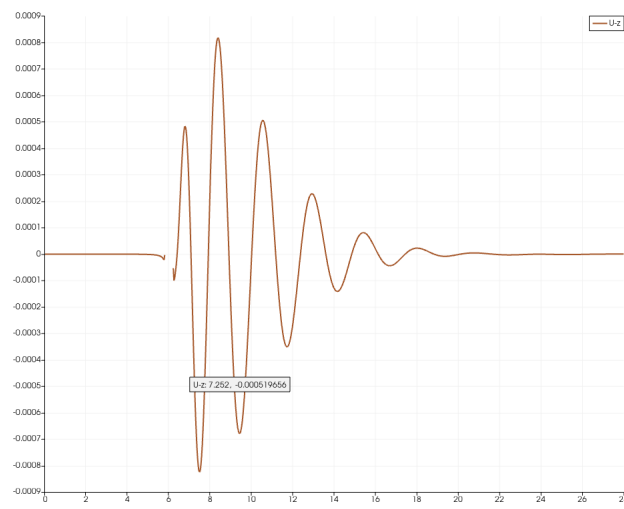


Figure 16:  $U-y$  for  $Re\ 1600$

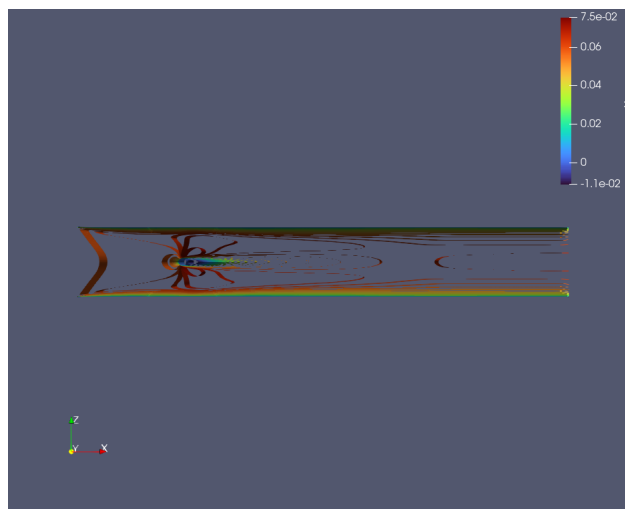


Figure 17:  $U-x$  Countour for  $Re\ 1600$

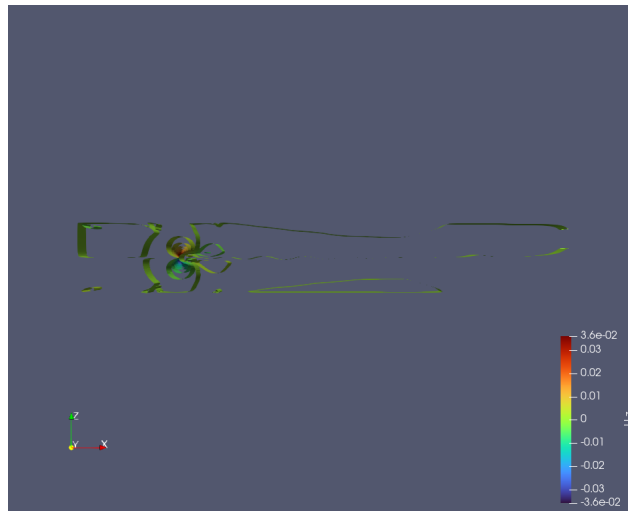


Figure 18: U-y Countour for Re 1600

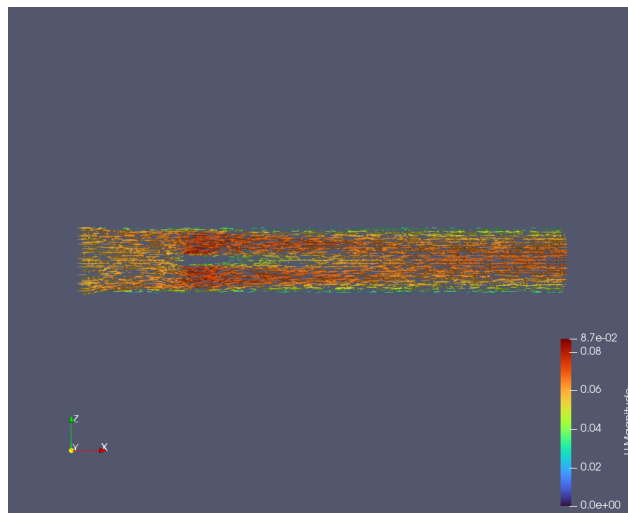


Figure 19: Vectors for Re 1600

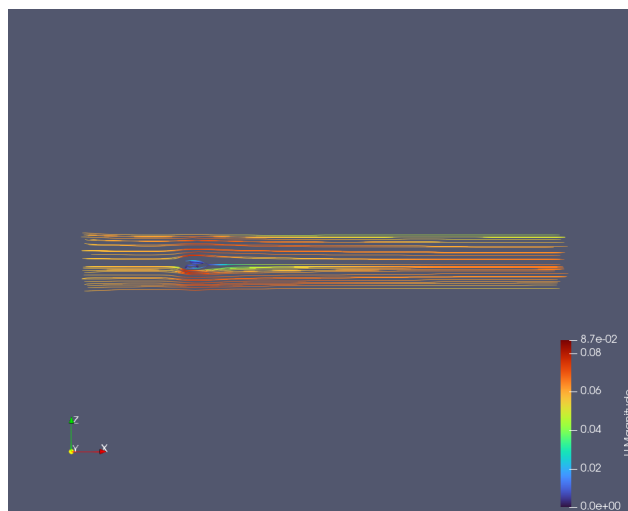


Figure 20: Streamlines for Re 1600

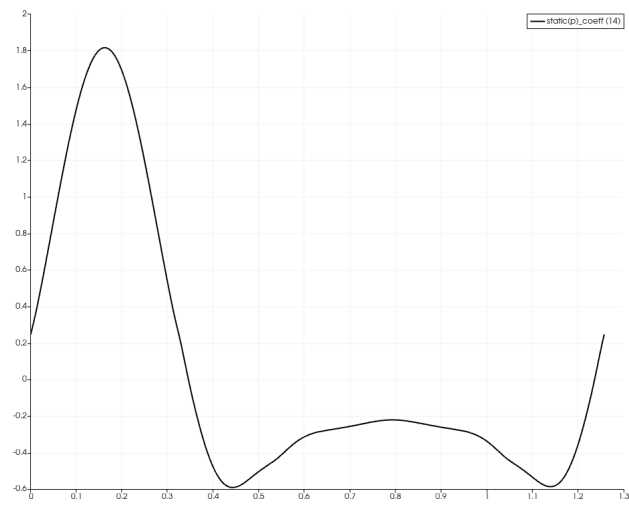


Figure 21: Pressure coefficient for Re 1600

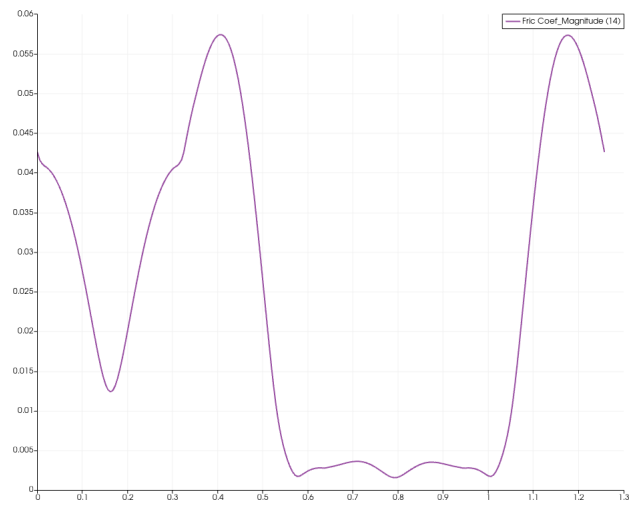


Figure 22: Friction Coefficient for Re 1600

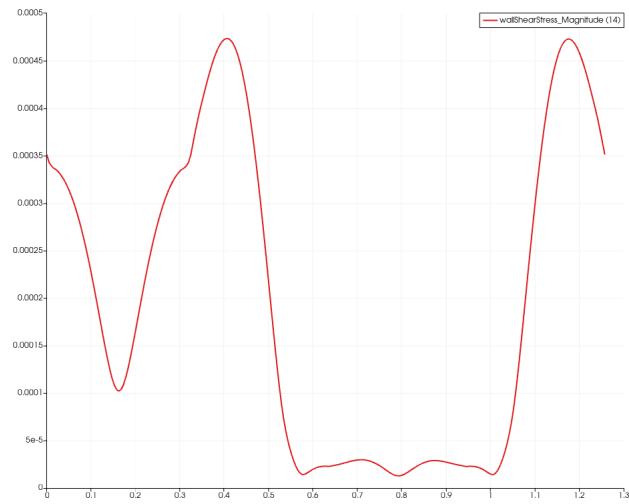


Figure 23: Wall Shear stress for Re 1600

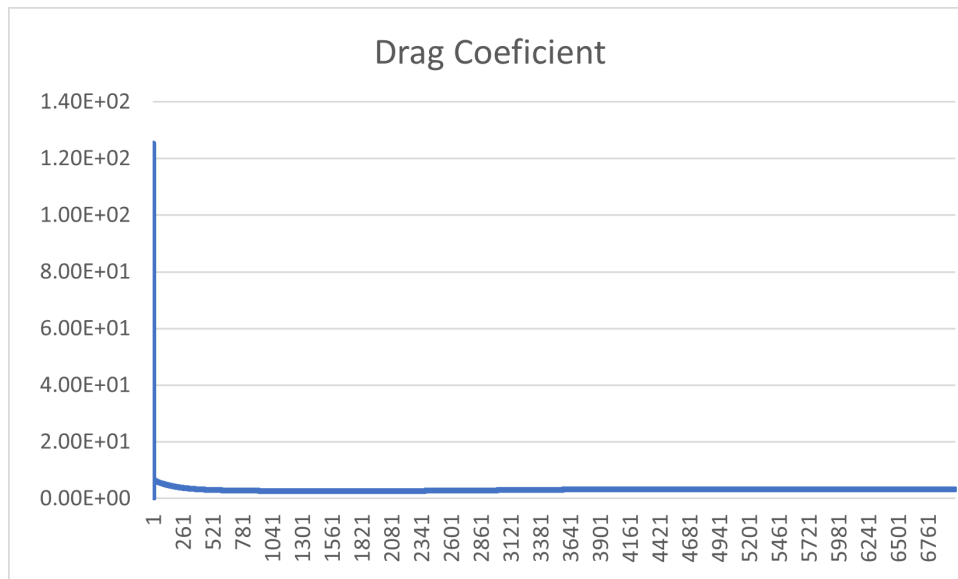


Figure 24: Drag Coefficient for Re 3900

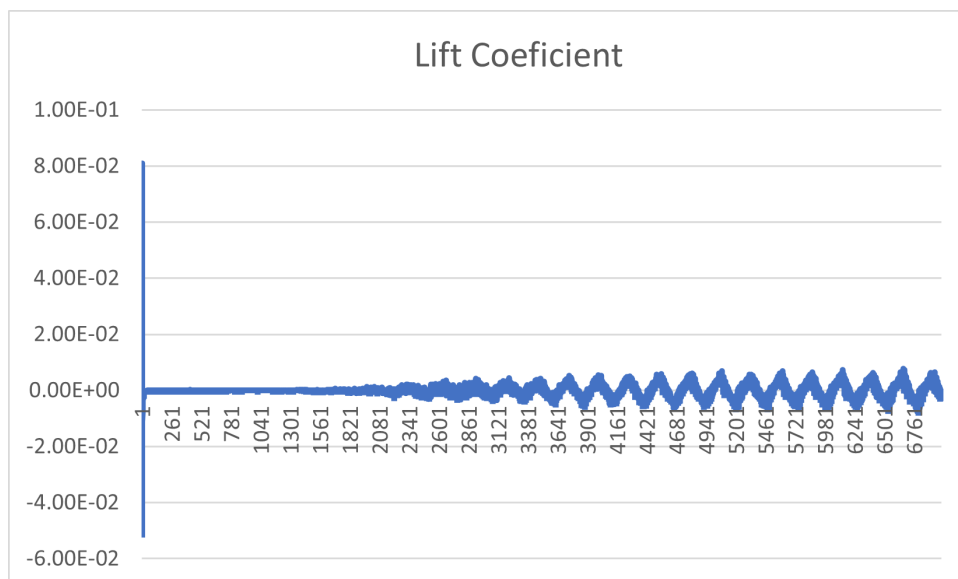


Figure 25: Lift Coefficient for Re 3900

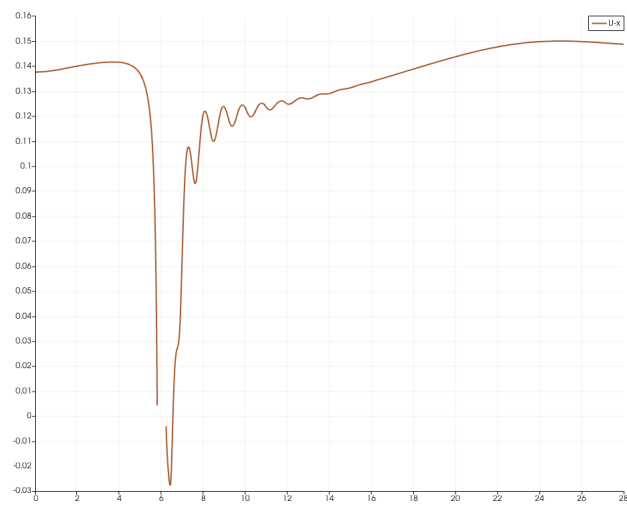


Figure 26:  $U-x$  for  $Re\ 3900$

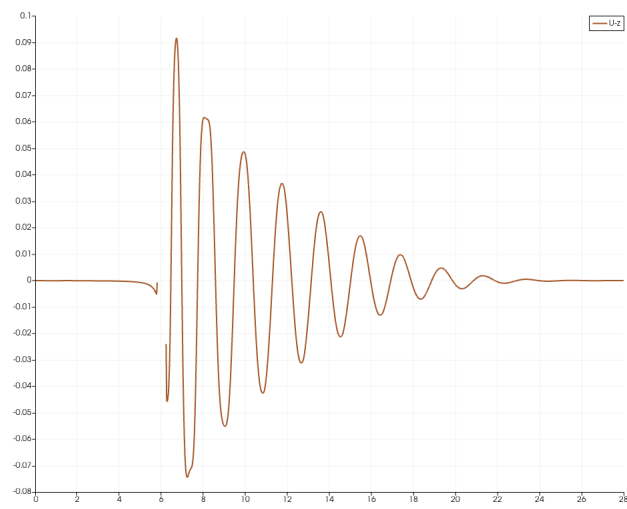


Figure 27:  $U-y$  for  $Re\ 3900$

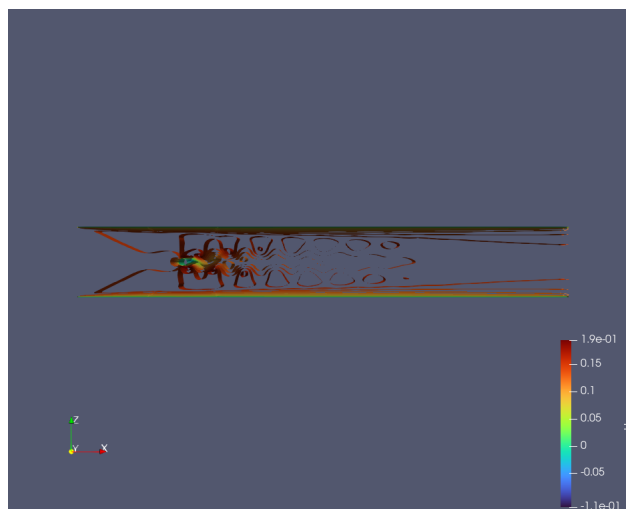


Figure 28:  $U-x$  Countour for  $Re\ 3900$



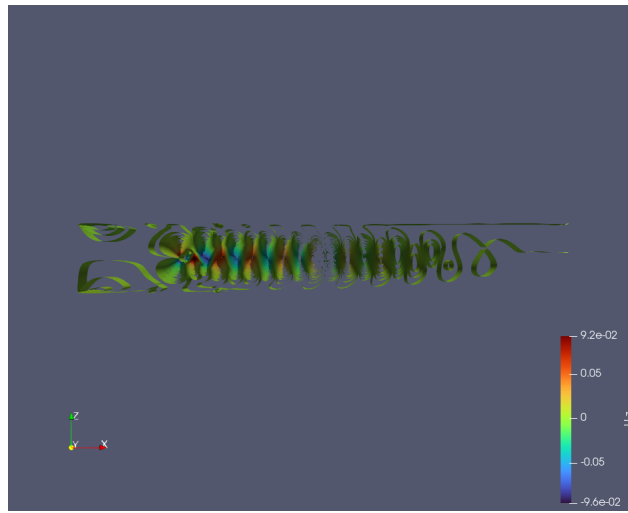


Figure 29: U-y Countour for Re 3900

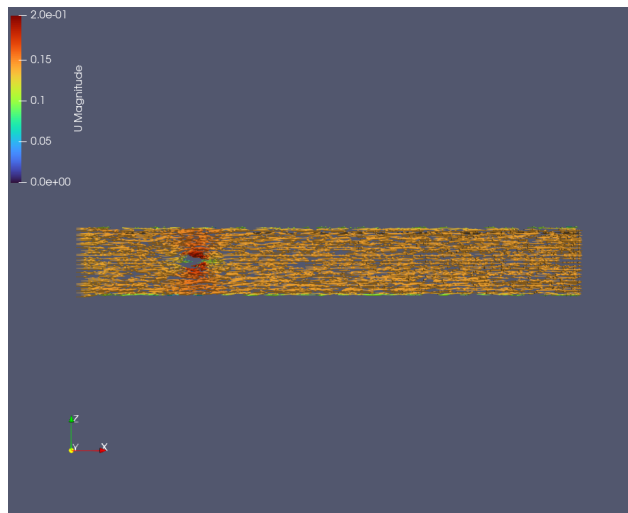


Figure 30: Vectors for Re 3900

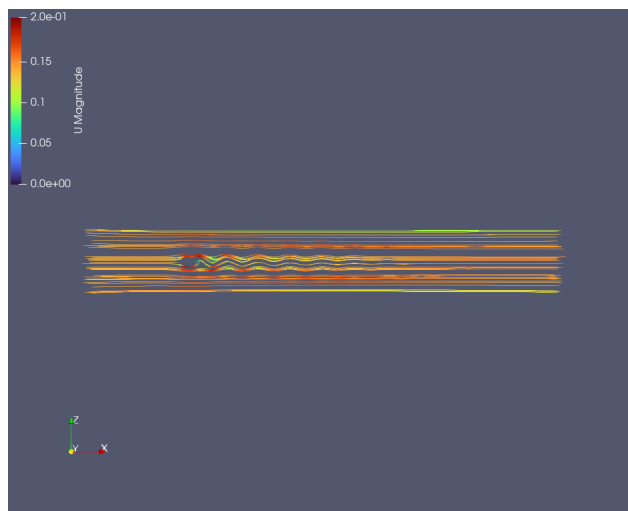


Figure 31: Streamlines for Re 3900

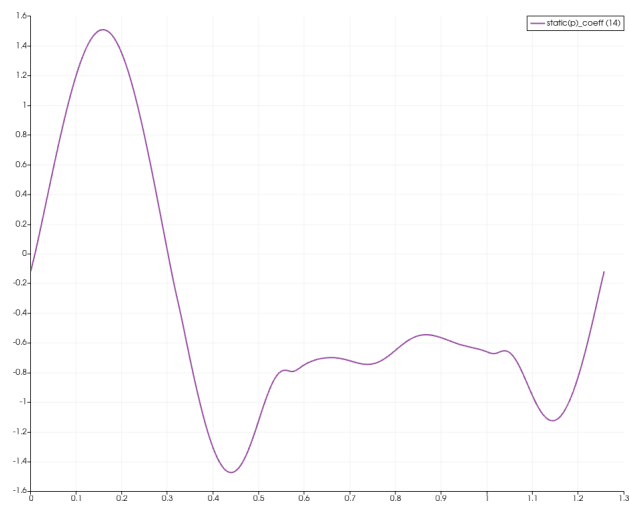


Figure 32: Pressure coefficient for Re 3900

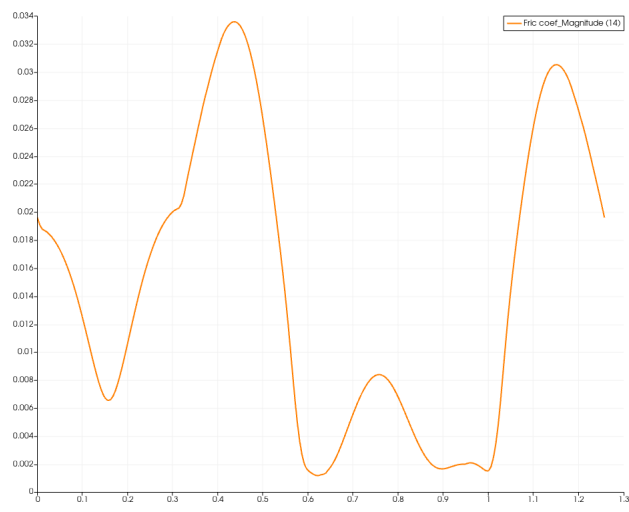


Figure 33: Friction Coefficient for Re 3900

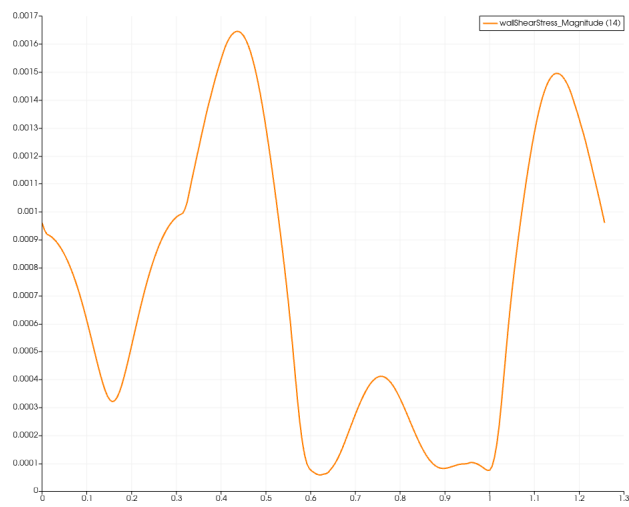


Figure 34: Wall Shear stress for Re 3900